CHAPTER 4

EVOLUTION OF COPPER OXIDE DAMASCENE STRUCTURES IN CMP: I. CONTACT MECHANICS MODELING

Non-planarity arising from the chemical mechanical polishing of Cu-oxide damascene results in the exposure field (die-size) being partially out of focus in the subsequent lithography process. The corresponding mechanisms for non-uniformity must be determined and minimized to increase the process yield. In this chapter, contact mechanics models are developed to explain the role of pattern geometry on the variation of material removal rate. The effects of Cu linewidth, area fraction, and the elastic properties of the polishing pad on pad displacement into low features are examined. The pressure distribution on the high features is determined and the rate of pattern planarization is quantified. Experiments on patterned Cu wafers are conducted to verify the model. Based on these results, the planarization and polishing behavior, and the within-die nonplanarity due to the pattern geometry variation are discussed.

4.1 Introduction

Continuing advances in ultra-large-scale integration (ULSI) necessitate the design and fabrication of extremely small devices. The existing metallization schemes for interconnects are inadequate for new circuits. It is projected that the RC delay due to metallization layers will account for 50% of the total circuit delay for CMOS circuits with gate dimensions less than 0.25 μm (Steigerwald et al., 1994). New materials and processes are needed to replace the present Al interconnects to reduce the RC delay and to decrease the energy loss due to heat dissipation. Copper has emerged as the favored interconnect material because of its lower electrical resistivity, about 30% less than that of Al. This allows ICs to operate at higher

speeds and lower power. Additionally, as interconnect dimensions are scaled down, the current density carried by the metal interconnects increases proportionally and might exceed the limit of eletromigration. The higher melting point Cu, however, provides a greater resistance to eletromigration, about 2.5 times greater than that of Al, thus dramatically increasing the reliability of the ICs. Despite the inherent advantage of Cu as an interconnect metal, several challenges are involved in the fabrication of copper lines. Because of the lack of volatile copper compounds at low temperature (less than 100 °C), copper etching to form the desired pattern on the top of the inter-level dielectric (ILD) layer is difficult. A damascene scheme involving trench patterning and deposition followed by CMP has demonstrated great potential for developments in the interconnect technology.

Figure 4.1 schematically shows the copper damascene structure. Copper and diffusion barrier layers (typically Ta, Ti or TaN) are deposited onto the etched inter-level dielectric (ILD) surface. Then CMP removes the excess Cu and forms conductive paths in the ILD trenches. The excess Cu coating is planarized at a rate related to the local pattern geometry (Murarka et al., 1993; Steigerwald et al., 1994; Park et al., 1999, Pan et al., 1999). The pattern within a die is slightly overpolished to remove all the Cu and barrier coating on the dielectric surface. Although this isolates the Cu interconnects, it also results in surface nonplanarity. The within-die nonplanarity might result in an exposure field (die-scale) partially out of focus for lithography. Overpolishing and dishing of the soft Cu surface also reduce the thickness of Cu interconnects and increase the electrical resistance. The corresponding mechanisms of planarization, dishing, and overpolishing must be determined and their impact on process yield must be addressed to best utilize the potential of Cu damascene polishing.

Much of the research on the effects of pattern geometry on material removal exclusively focused on ILD (SiO_2) polishing (Warnock, 1991; Burke, 1991; Runnels, 1994 and 1996; Boyd and Ellul, 1996; Stine et al., 1997; Ouma et al., 1997). Nevertheless, the results of ILD polishing can be adapted to the planarization stage in metal polishing because the pattern geometries are similar. The only difference is the material polished. Warnock, 1991 proposed a phenomenological model to relate the polishing rate of arrays of various features

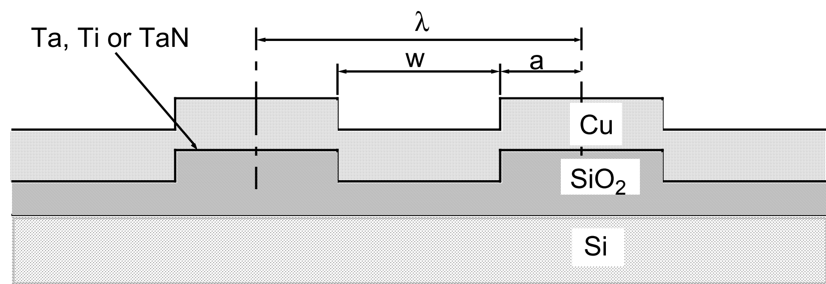

(a)

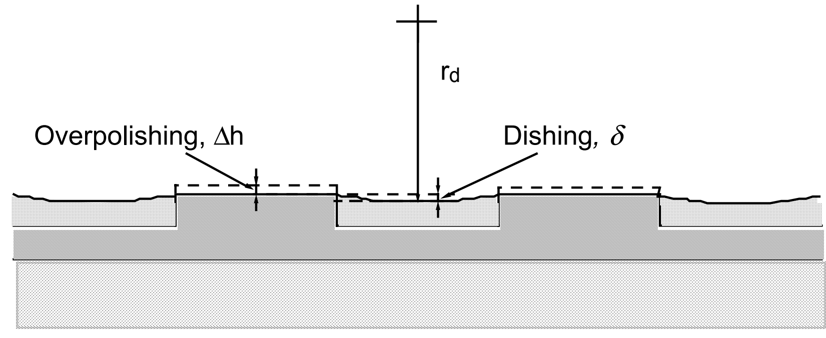

(b)

Figure 4.1 Schematics of Cu damascene structure: (a) before polishing, and (b) after polishing.

to the feature dimension and pattern density. He predicted the surface profile evolution by experimentally determining the correlation between the polishing rate, feature dimensions, and the neighboring feature layout. However, the correlation between the polishing rate and pattern geometry varies with different pattern design, and the tribological mechanisms of planarization are left unanswered in this model. Recently, the effects of pattern geometrical parameters, such as pattern density (i.e., high feature area fraction), pitch, pattern area, and the ratio of perimeter to area, were extensively studied (Stine et al., 1997). It is shown that the pattern density significantly affects the subdie-scale polishing. The influential range of a specific pattern on a neighboring area was characterized by a planarization length measured experimentally. A density-based numerical model was proposed to characterize the surface topography evolution for arbitrary layouts. Experiments were also conducted to verify this model (Stine et al., 1997; Smith et al., 1999).

On the theoretical side, contact mechanics models have examined the mechanisms of planarization. A planar elastic pad was assumed for predicting the pressure distribution on the die surface with various pattern layouts (Chekina et al., 1998; Chen and Lee, 1999). A generalized relation between pressure distribution and the pad displacement was proposed. An analytical solution for pattern evolution in steady-state regimes was also presented by Chekina et al. Based on the model, the nonunifom polishing rate across different pattern regions is attributed to the nonuniform pressure on the high features. The low features were assumed to stay intact until the deformed pad contacts them. However, the steady-state analysis might be not applicable for some pattern layouts in Cu polishing. The pad might be in contact with the low features before the high features reach the steady-state profile. Additionally, the pad might not conform to the high features as assumed in this model.

This chapter proposes models for different polishing regimes of metals. Contact mechanics models, with conformal and non-conformal elastic pads, are employed for the planarization regime. The effects of the pattern geometry (linewidth and area fraction) and the pad elastic properties on the pressure distribution and pad displacement are investigated to explain the variation of MRR on different patterns and the evolution of surface profile. These contact mechanics models are examined by polishing patterned test wafers. The understanding of nonplanar polishing due to pattern geometry will enlighten the study of Cu

dishing and oxide overpolishing. Steady-state dishing and overpolishing will be modeled and examined experimentally in Chapter 5. Accordingly, the fundamentals of Cu damascene polishing and the mechanisms of within-die nonuniformity of material removal are examined and the important process parameters are identified.

4.2 Theory: Contact Mechanics Modeling

Local pattern geometry affects pressure distribution *p(x,y)* and thus results in a nonuniform material removal according to the Preston equation (Preston, 1927):

$$\frac{dh}{dt} = k_p p(x, y) v_R \,. \tag{4.1}$$

where h is the thickness of the layer removed, t the polishing time, v_R the relative velocity, and k_p the Preston constant. The objective of contact mechanics modeling, then, is to determine the pressure distribution on the feature surface. As shown schematically in Fig. 4.2, three regimes of polishing of patterned wafers may be postulated: planarization, polishing, and dishing/overpolishing. In the planarization regime in Figs. 4.2 (a) and 4.2 (b), the step-height between the high and low features is much larger than the pad displacement u_z and hence the load is essentially supported by the high features. The contact mechanics models determine the pressure variation on high features as well as the pad displacement outside the high features to ensure no wafer/pad contact on the low features. As the pad contacts the low area, however, both high and low features will be polished concurrently. The pressure distribution will become ever more uniform as the surface is being gradually smoothed down, Fig 4.2 (c). In this regime, the thin, planar Cu layer is polished as in blanket polishing. When the Cu layer is polished through with a planarized surface, the pressure on both Cu and oxide would be about the same. As shown in Fig. 4.2 (d), the soft interconnect Cu now wears faster than the diffusion barrier layer (Ta, Ti or TaN) and the ILD. The surface of Cu interconnect is dished. Additionally, the oxide will be overpolished with the increase of overpolishing time, which may deteriorate surface planarity.

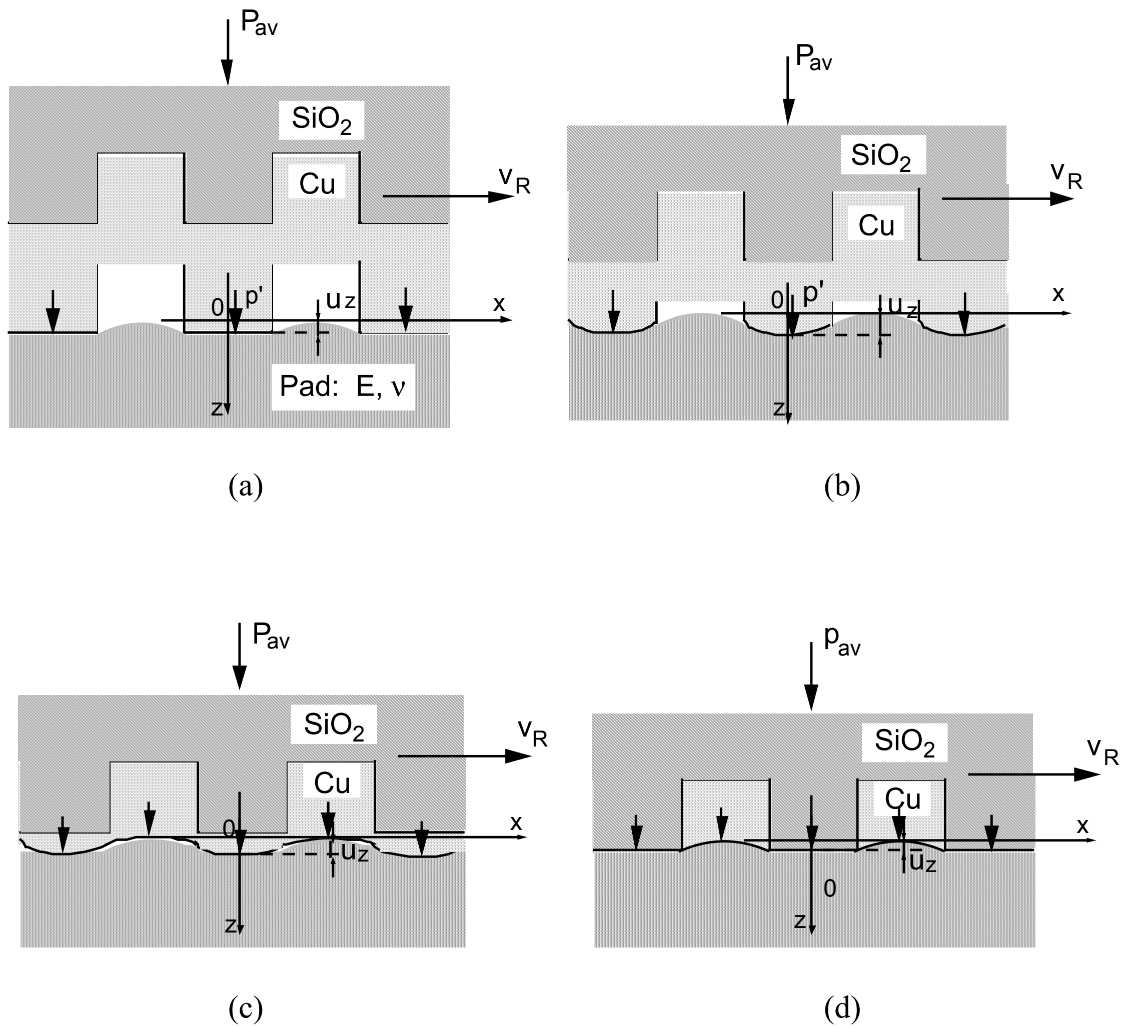

Figure 4.2 Schematics of the pattern/pad contact interface: (a) initial stage with uniform displacement specified on high feature, (b) planarization stage with pressure specified (either uniform pressure or elliptical distribution) on the contacting high features, (c) end of the planarization with pad in contact with low area, and (d) the onset of dishing and overpolishing.

4.2.1 Geometry and Boundary Conditions. Consider a rigid line structure on the wafer in contact with the elastic pad as shown in Fig. 4.3. The high features (shaded in Fig. 4.3) represent the Cu deposited on the underlying oxide and the low areas represent the Cu fill in the trenched oxide region. Because the length of the line is much greater than its lateral dimensions, the pattern/pad contact can be modeled as a two-dimensional (plane-strain) problem. The pad deformation is usually much smaller than the pad thickness. Thus the contact stresses are highly concentrated near the pad surface. With this approximation, the stresses can be calculated by assuming the pad as an elastic semi-infinite body. Now the boundary conditions along the pad surface must be specified to solve the stress and strain field in the elastic pad. On the boundary outside the loaded region, the surface is free of stress, i.e.:

$$\sigma_z = \tau_{xz} = 0, \ |x| > a \tag{4.2}$$

Within the loaded region, for simplification, the tangential traction will be assumed to be negligible in the following analysis, i.e.:

$$\tau_{xz} = -q(x) = 0, \quad -a < x < a \tag{4.3}$$

This assumption stands only when the friction coefficient at the wafer/pad contact interface is low. Prior experimental results confirm that the friction coefficient in Cu polishing is about 0.1. Therefore, the effect of tangential traction on the stresses is negligible. Additionally, the normal stress within the loaded region can be specified to determine the pad tangential and normal displacements $u_x(x)$ and $u_z(x)$ on the entire surface, i.e.:

$$\sigma_z = -p(x), \quad -a < x < a \tag{4.4}$$

This problem has been solved in the contact mechanics literature. The formulation of the pad displacements within the contact region may be expressed in differential forms (Galin, 1961; Johnson, 1985):

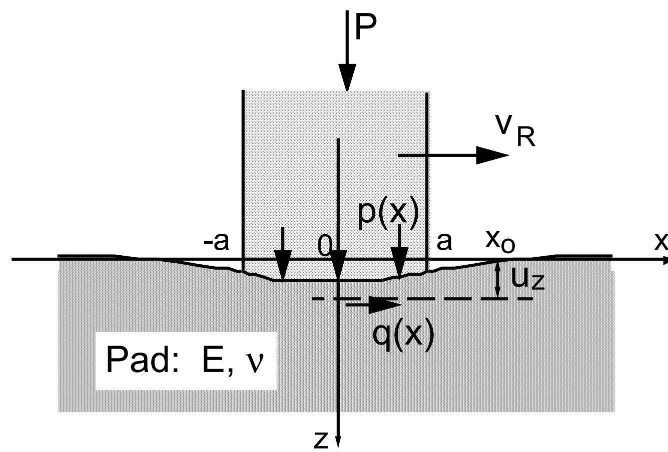

Figure 4.3 Schematic of a moving rigid line structure in contact with a elastic pad.

$$\frac{\partial u_x(x)}{\partial x} = -\frac{(1-2\nu)(1+\nu)}{E} p(x) \quad (4.5a)$$

$$\frac{\partial u_z(x)}{\partial x} = -\frac{2(1-\nu^2)}{\pi E} \int_{-a}^{a} \frac{p(s)}{x-s} ds \quad (4.5b)$$

where ν is the Poisson's ratio, E the Young's modulus of the pad, and s a dummy variable.

4.2.2 Uniform Pressure Distribution. The boundary condition of uniform pressure may be applied when a steady-state profile of high features is reached without contact on the low features, Fig. 4.2 (b). The pressure distribution can be related to the load P on each high feature $|x - n\lambda| \leq a$ and the half width a of the feature as:

$$p(x) = \frac{P}{2a} \quad (4.6)$$

where P is the force per unit length on each contact region, n the index of the high feature from the center of the specific area (from -N to N, totally $2N$+1 high features). Equation (4.6) assumes the load P on the high features to be constant. This would be true when the features of interest are near the center of a specific pattern area with constant linewidth and pitch. Thus its pressure distribution would not be affected by the different pattern in the neighboring sub-die area. Utilizing this boundary condition, Eq. (4.5b) can be solved for the pad displacement over the specific area. The displacement of the pad can be written in normalized form as:

$$\bar{u}_z(x) = -\frac{(1-\nu^2)}{\pi E} \frac{P}{2a} \sum_{n=-N}^{N} \left[\left(1 + \frac{x-n\lambda}{a}\right) \ln\left(1 + \frac{x-n\lambda}{a}\right)^2 + \left(1 - \frac{x-n\lambda}{a}\right) \ln\left(1 - \frac{x-n\lambda}{a}\right)^2 \right] + (2N+1)C_2 \quad (4.7)$$

where $\bar{u}_z(x)$ is the normalized displacement of the pad along the surface, defined as $\bar{u}_z(x) \equiv u_z(x)/a$, and C_1 is an integration constant and determined relative to a datum x_o.

$$C_1 = \frac{(1-\nu^2)}{\pi E}\frac{P}{2a}\left[\left(1+\frac{x_o}{a}\right)\ln\left(1+\frac{x_o}{a}\right)^2 + \left(1-\frac{x_o}{a}\right)\ln\left(1-\frac{x_o}{a}\right)^2\right] \tag{4.8}$$

The datum x_0 is arbitrarily chosen on the displaced surface referred to the initial surface plane, in which $u_z(x_o) = 0$. The choice of x_o usually refers to the observation on the real deformed surface. The difficulty of determining C_1 is a general feature of elastic half-space problems because the conditions far away from the contacting surface are undefined. To surmount the difficulty, the actual shape and dimension of the elastic body and the boundary conditions at the supporting sides must be considered. However, if interest is on the relative shape of the pad surface and its displacement into low features instead of the movement of its surface level, the choice of x_o is unimportant and will not affect the profile of the pad surface.

4.2.3 Elliptical Pressure Distribution. Another possible boundary condition on the high feature is an elliptical pressure distribution given by the Hertz theory. In this case, both the wafer and the pad are modeled as non-conforming elastic bodies. The pressure distribution in the contact region, $|x - n\lambda| \le a$, can be expressed as (Johnson, 1985):

$$p(x) = p_o\left(1-\left(\frac{x}{a}\right)^2\right)^{1/2} \tag{4.9}$$

where p_o is maximum pressure on the feature and can be found by:

$$p_o = \frac{2P}{\pi a} \tag{4.10}$$

As shown in Fig. 4.4, the pressure distribution can be rewritten as the normalized form, $\overline{p}$ (where $\overline{p}(x) \equiv 2ap(x)/P$), versus the dimensionless distance, x/a.

$$\overline{p}(x) = \frac{4}{\pi}\left(1-\left(\frac{x}{a}\right)^2\right)^{1/2} \tag{4.11}$$

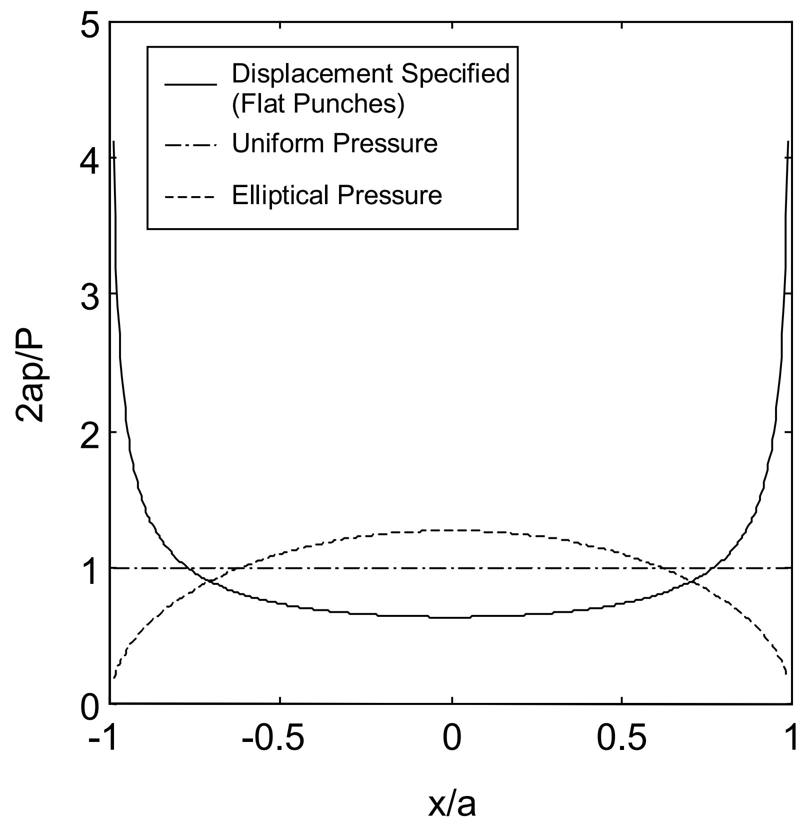

Figure 4.4 Pressure distribution in the contact region of the high feature for various boundary conditions.

The elliptical pressure distribution should result in a higher rate of material removal near the center of the high features. However, this will change the profile of the high features quickly and promote the pressure distribution toward a more uniform fashion. Applying this elliptical pressure distribution on the boundary, the normalized displacement is given as:

$$\bar{u}_z = -\frac{4(1-\nu^2)}{\pi E}\frac{P}{2a}\sum_{n=-N}^{N}\left\{\left(\frac{x-n\lambda}{a}\right)^2 - \left[\frac{|x-n\lambda|}{a}\sqrt{\left(\frac{x-n\lambda}{a}\right)^2-1} - \ln\left(\frac{|x-n\lambda|}{a}+\sqrt{\left(\frac{x-n\lambda}{a}\right)^2-1}\right)\right]\right\} + (2N+1)C_2 \quad (4.12)$$

where C_2 is another dimensionless integration constant.

$$C_2 = \frac{4(1-\nu^2)}{\pi E}\frac{P}{2a}\left\{\left(\frac{x_o}{a}\right)^2 - \left[\frac{|x_o|}{a}\sqrt{\left(\frac{x_o}{a}\right)^2-1} - \ln\left(\frac{|x_o|}{a}+\sqrt{\left(\frac{x_o}{a}\right)^2-1}\right)\right]\right\} \quad (4.13)$$

4.2.4 Rigid Flat Punches with Specified Displacement. In some cases, it may be simpler to specify the normal displacement $u_z(x)$ instead of the pressure distribution within the contact region on the assumption that the pad conforms to the profile of the high feature. The solution for this "mixed boundary-value problem" is also given in the contact mechanics literature (Galin, 1961). The general solution of the singular integral equation for $p(x)$, Eq. (4.5b), in the contact region is given by:

$$p(x) = -\frac{E}{2(1-\nu^2)(a^2-x^2)^{1/2}}\int_{-a}^{a}\frac{(a^2-s^2)^{1/2}}{(x-s)}\frac{\partial u_z(s)}{\partial s}ds + \frac{P}{\pi(a^2-x^2)^{1/2}} \quad (4.14)$$

For example, the pattern profile is known from the prior deposition process in the initial stage of Cu planarization, as shown in Fig. 4.2 (a). By assuming uniform indentation ($\partial u_z/\partial x = 0$) across the flat loaded region, the pressure distribution on an array of high features $|x-n\lambda| \le a$ can be obtained from Eq. (4.14) as:

$$p(x) = \frac{P}{\pi\left[a^2 - (x - n\lambda)^2\right]^{1/2}} \tag{4.15}$$

Figure 4.4 also shows the normalized pressure $\overline{p}$ versus the normalized distance *x/a* across a high feature for the flat-punch contact. The pressure reaches a theoretical infinite at the edges of the high features due to the discontinuity in $\partial u_z/\partial x$. In practice, a finite radius retains the continuity of $\partial u_z/\partial x$ across the edge. The pressure would increase to a high but finite value. Moreover, because the pad material cannot sustain such a high stress, it yields plastically. Thus the pressure would not be higher than the yield/fracture strength of the pad. Despite the pressure concentration near the edges, the pressure is distributed more or less uniformly over the feature at close to about 0.7 times the average pressure *P/2a* in the contact region. Increase of the load on each high feature proportionally increases the pressure at each point but dose not change its distribution. Equation (4.15) shows that the general shape of the curve is not affected by the elastic properties of the pad.

The pad displacement outside the high features is found by substituting the pressure within loaded regions obtained from Eq. (4.15) into Eq. (4.5b) and by performing the integration. The pad displacement can be expressed in the normalized form as:

$$\overline{u}_z(x) = -\frac{4(1-\nu^2)}{\pi E}\frac{P}{2a}\sum_{n=-N}^{N}\ln\left[\frac{x-n\lambda}{a} + \left(\left(\frac{x-n\lambda}{a}\right)^2 - 1\right)^{1/2}\right] + (2N+1)C_3 \tag{4.16}$$

where C_3 is the normalized integration constant, defined in the case of single flat punch indentation as:

$$C_3 = \frac{2(1-\nu^2)}{\pi E}\frac{P}{2a}\ln\left[\frac{x_o}{a} + \left(\frac{x_o^2}{a^2} - 1\right)^{1/2}\right] \tag{4.17}$$

4.3 Results

4.3.1 Pad Displacement. Figure 4.5 plots the normalized pad displacements for the various boundary conditions based on Eqs. (4.7), (4.12), and (4.16). The zero on the ordinate refers to the bottom of the high features. The displacement is calculated based on the geometry and conditions close to current CMP practice. The area fraction is 0.5 ($A_f = w/\lambda = 1- 2a/\lambda = 0.5$), and the applied pressure on the wafer is 50 kPa (7 psi). As shown in Table 4.1, the elastic modulus and Poisson's ratio of the pad are assumed to be E = 500 MPa and ν = 0.3 (close to those of the bulk commercial pads), respectively. However, for features with dimensions smaller than the sizes of pad asperities (about 20–50 μm), the intrinsic elastic properties of the pad material may be employed to calculate the pad displacement. Since the intrinsic Young's modulus of the pad is higher than that of the porous pad (e.g. about 1.18 times higher for the pad with 15% of porosity in volume), the use of bulk properties will result in overestimation of the pad displacement for the small lines (about 18%). Table 4.1 shows the properties of the materials being polished. The assumption of rigid punch indentation in prior analyses is valid since the Young's moduli of all materials involved in Cu damascene pattern are much high than that of the pad.

The maximum displacements of the pad for the three boundary conditions are of approximately the same order of magnitude. For current circuit design, in which the width of small features is about w = 0.18 - 0.5 μm (or a = 0.09 - 0.25 μm for features with area fraction of 0.5), the displacement of the pad outside the high features is about 0.03 to 0.08 nm, almost negligible compared with the surface roughness of the pad. Therefore, if the step-height is much larger than the pad displacement, as in the planarization stage of Cu polishing (for an initial step-height of about 0.5 - 1 μm), the pad will not be in contact with the low surfaces. Thus the material removal rate on the low features will be relatively low because no abrasion occurs until the end of the planarization process. Additionally, the within-die nonplanarity will result in a variation of the average pressure on different patterns, affecting the pad displacement. The pressure distribution on different high features at the nonplanar surface can be determined numerically based on Eq. (4.5) with a displacement specified boundary condition in the contact region corresponding to the actual surface topography. The experimental results show, however, the effect of mean pressure variation due to within-die

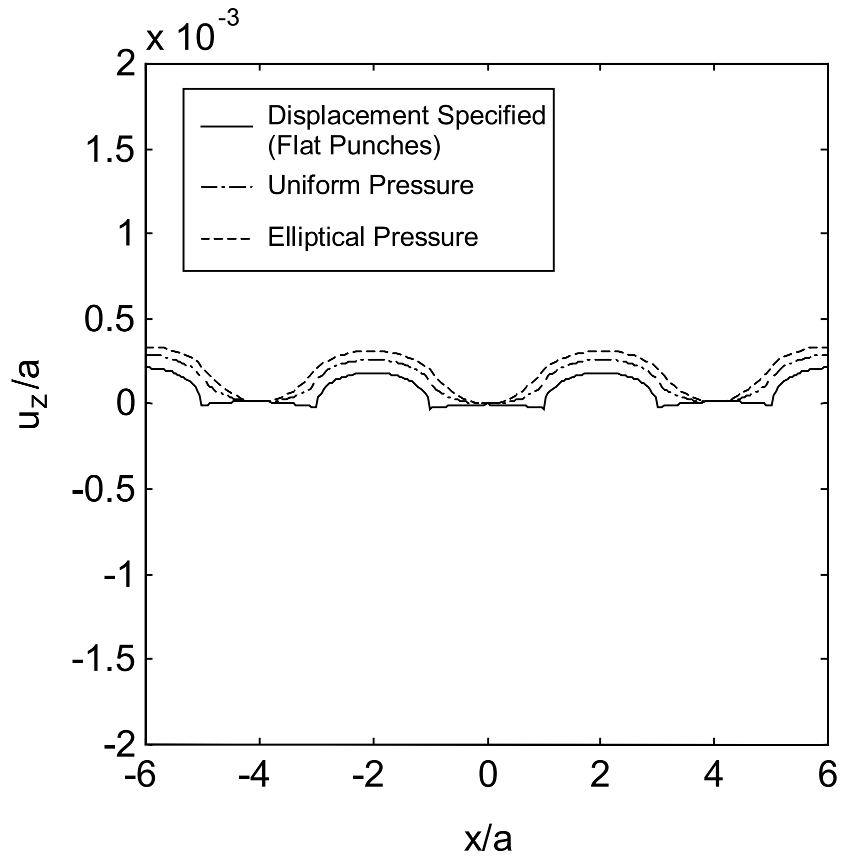

Figure 4.5 Surface Profiles of deformed pad for various boundary conditions.

Table 4.1: Elastic properties of materials.

Material	Young's Modulus (GPa)	Poisson's Ratio
Cu	128[†]	0.30
Ta	186[†]	0.30
SiO_2 (TEOS)	74[††]	0.20
Rodel Pad	0.5	0.30

[†] ASM Metals Handbook, ASM International.
[††] Handbook of Materials Science, CRC Press Inc.

nonplanarity is not as significant as the local pattern geometry, linewidth, and area fraction on the pad displacement.

4.3.2 Effect of Pattern Linewidth. The effects of linewidth on pad displacement are also illustrated in Fig. 4.5. For a pattern with constant area fraction, such as 0.5, the increase of linewidth will proportionally scale up the displacement of the pad. Consequently, the pad might start to contact the low area before the topography is planarized. For instance, the pad displacement is about 20 nm for a 100 μm wide line. When the size of pad asperities, about 100 - 200 nm, and particle size, about 200 nm, are taken into consideration, the low area of a wide feature (interconnect line, contacting pad) will be in contact with the pad/particle in the planarization regime (about half of the initial step-height in this case). By contrast, for sub-micron size features, the pad asperities cannot reach the low feature freely giving the constraint of the surrounding high features. Hence, the pad does not contact the low area until the end of the planarization regime.

Increased linewidth for the same A_f also decrease the (average) MRR on the high feature. Because part of the load at some point in the planarization regime is supported by the low features, the average pressure on the high feature decreases as does the MRR. The variation of the MRR for different area fraction regions causes a variation of process duration for clearing Cu. This results in part of the die being overpolished and introduces oxide thickness variation and Cu loss problems. Additionally, the sooner the low features are in contact with the pad, the more likely that the surface topography is partially retained until the end-point of the process. This may increase surface nonuniformity and start dishing the Cu in the trenches before the Cu layer is polished through. Dishing and overpolishing will be addressed later in the Chapter 5.

4.3.3 Effect of Pattern Area Fraction. The effects of area fraction are shown in Fig. 4.6. The normalized pad displacement, u_z/a, increases with the A_f. The three boundary conditions show the same trends and similar displacement values. Among the three, the elliptical pressure distribution yields the largest pad displacement for all A_f. For lower A_f, the uniform pressure boundary condition results in a slightly larger pad displacement in the low area than that of the (constant) displacement specified condition. When A_f is greater than

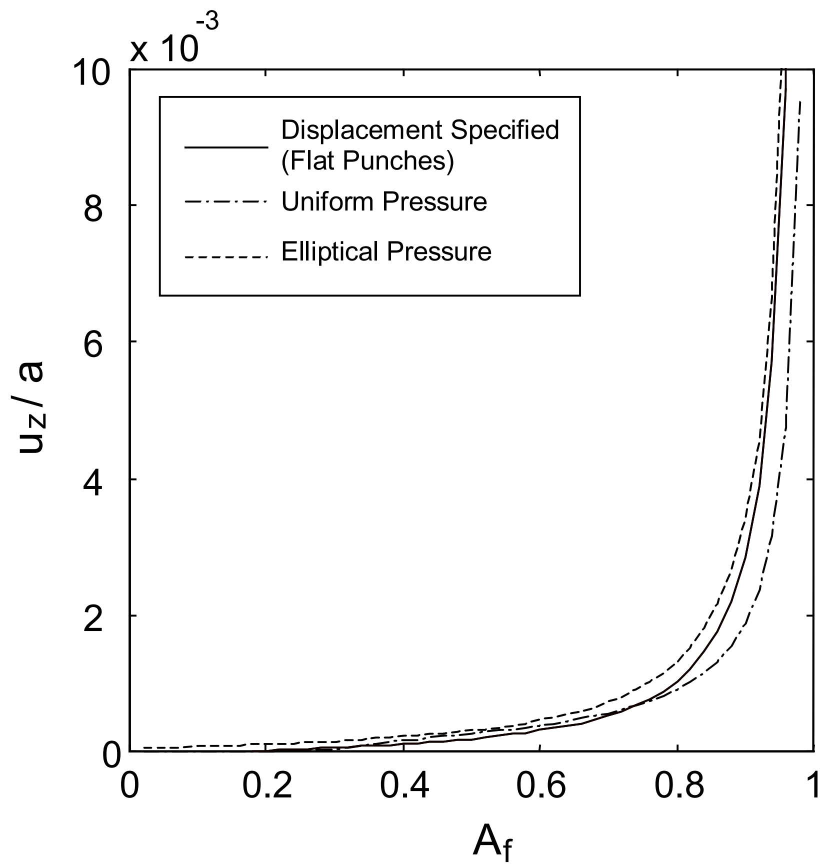

Figure 4.6 Pad displacement versus pattern area fraction for various boundary conditions.

approximately 0.7, the pad displacement is more in the low area for the boundary condition of specified displacement in the loaded region.

Except for the steep increase of u_z/a with A_f at higher area fraction regions, i.e. greater than 0.7, the displacement increases almost linearly with A_f. Between the area fractions of 0.2 to 0.6, the slope of the curve is about $1x10^{-3}$. Thus the pad displacement will be about the same order of magnitude even with a slight variation of area fraction for the present circuit designs. Therefore, for the first few metal layers with fine interconnects, the surface will be planarized before the pad contacts the low area. Moreover, if the Cu linewidth is small and the effect of pad displacement is essentially negligible, the MRR and the rate of planarization will both increase proportionally with A_f because the average pressure on the high features is inversely proportional to A_f. This will result in build up the surface non-planarity within the die across different area fraction regions in the planarization stage of process.

4.3.4 Effect of Pad Elastic Properties. The effect of pad elastic modulus is shown in Fig. 4.7 with a dimensionless parameter p_{av}/E, which is close to 10^{-4} for the present pad and the nominal pressure employed in CMP. However, different pads may vary the degree of surface planarity. For example, some engineering plastics, with E about an order of magnitude greater than the polyurethane pad (about 1-5 GPa), or even some soft metals, with a two-order-of-magnitude greater E (about 10-20 GPa), could improve the surface planarity. Figure 4.7 indicates that the pad displacement will decrease proportionally with the increase of E or the decrease of p_{av}/E value. The results can be applied to the pad displacement at both the low feature and the lower subdie region which has been polished down faster than the surrounding low area fraction region due to higher area fraction. By using a stiffer pad, the surface level of two distinct area fraction regions may be maintained at a small difference and retain the surface planarity across the die. On the other hand, a compliant pad, such as some polymer foams with E ranging from close to the present pad (about 500 MPa) down to one order magnitude less (about 10 MPa), may be employed in the final polishing regime to reduce the load on abrasive particles and prevent surface scratching. The contact mechanics models can determine the desired range of pad properties with respect to the range of applied pressure to satisfy the requirements at different process regimes.

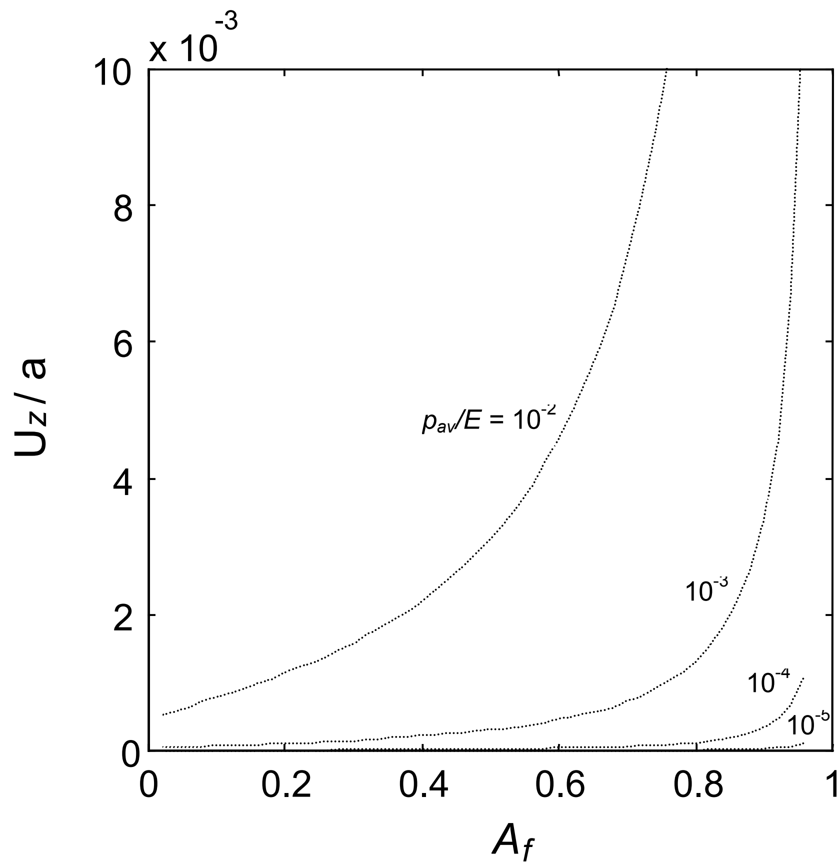

Figure 4.7 Effects of applied pressure p_{av} and Young's modulus of the pad E on the pad displacement (elliptical pressure distribution).

4.4 Experimental Validation and Discussion

4.4.1 Experimental Conditions. As shown in Fig 4.8, a Cu damascene structure was designed to verify the results of contact mechanics modeling. The pattern for each die (10 mm x 10 mm) consists of a matrix of 2.5 mm x 2.5 mm blocks (sub-die). These blocks in turn consist of line-space features, whose dimensions are close to the scale of the Cu interconnects on current chips with a minimum linewidth of 0.5 μm and a maximum linewidth of 100 μm. The area fraction of the experimental mask ranges from 0.01, representing an isolated line, to 0.5, representing a dense packing case. This pattern is transferred into a 2 μm thick SiO_2 coating by lithography on a 100 mm, (100) orientation silicon wafer. After oxide trenches are etched to a depth of 1 μm, a 20 nm thick Ta barrier layer is deposited, followed by a 1.5 μm thick Cu film. The mask layout and the corresponding area fractions of metal interconnect lines with respect to the specific w and λ are shown in Fig 4.8.

In this set of experiments, low nominal pressure of 28 kPa (4 psi) and linear velocity of 0.46 m/s were employed to decrease the MRR for a period of planarization longer than the normal CMP conditions. A neutral slurry with 4 vol.% of 0.3 μm Al_2O_3 abrasive particles allowed focus to remain the mechanical aspect of the process. The polishing experiments were conducted on the grooved commercial polyurethane pad, Rodel IC-1400. Conditioning was performed between each polishing to retain a similar surface condition of the pad. The initial and polished profiles of the patterns were recorded by a stylus profilometer and an atomic force microscope (AFM), for coarse and fine structures respectively.

4.4.2 The Evolution of Patterns. Figure 4.9 shows the evolution of the patterned surface (w = 5 μm and λ = 500 μm). Due to the high reflectance of Cu, the unpolished, scratch-free high features appear bright in the optical micrograph, Fig. 4.9 (a). The walls between the high and low surfaces appear dark in bright-field illumination because less normal incident light is reflected. The low features are less reflective because of the coarse microstructure from the Cu deposition. After two minutes of polishing as shown in Fig. 4.9 (b), the surface of the high features was slightly roughened, but still highly reflective in comparison to the low area. The same coarse microstructure and scratch-free surface of the

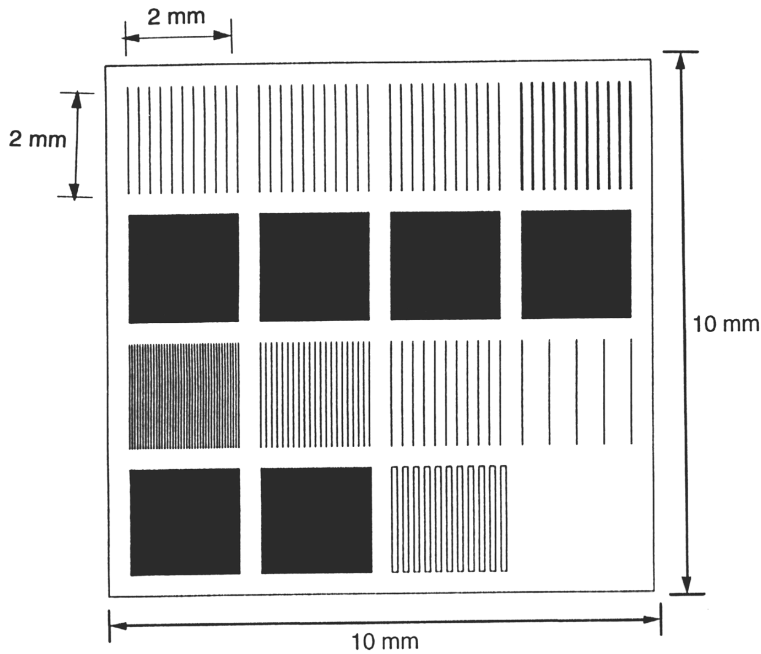

0.5/200 0.0025	0.7/200 0.0035	5/200 0.025	25/200 0.125
0.5/1 0.5	0.5/2 0.25	0.5/4 0.125	0.5/10 0.05
0.5/50 0.001	1/100 0.01	2/200 0.01	5/500 0.01
2/4 0.5	25/50 0.5	100/200 0.5	Field (No feature)

Linewidth (μm) / Pitch (μm)
Area Fraction

(a) (b)

Figure 4.8 Schematics of the CMP mask: (a) mask layout, and (b) pattern geometry layout.

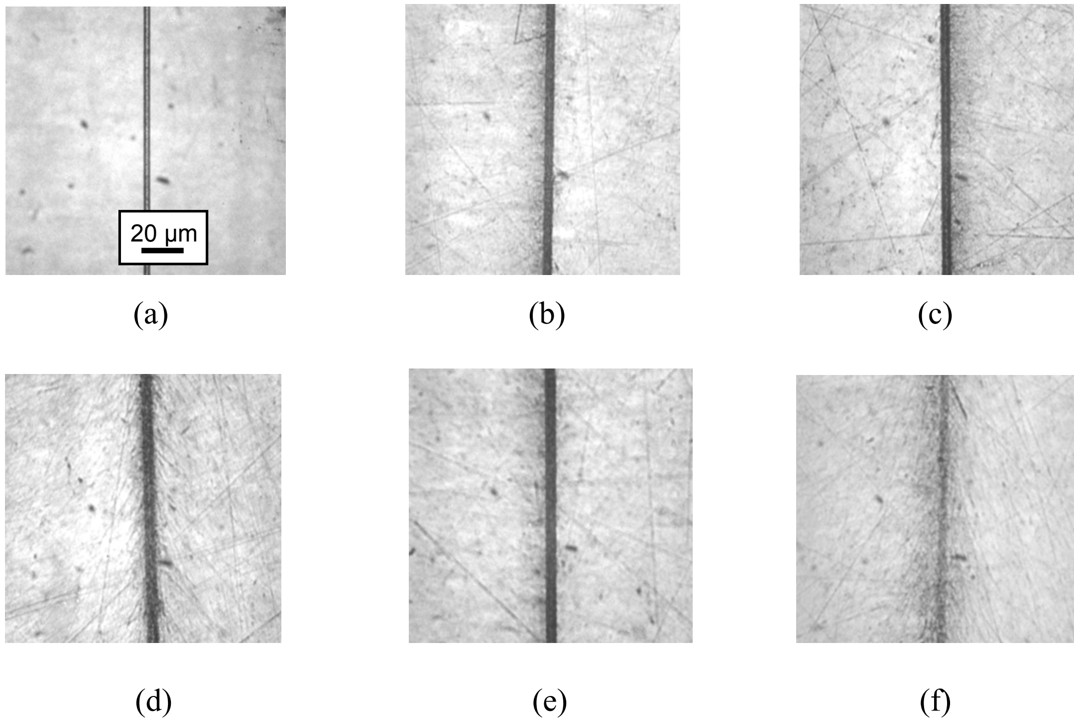

(a) (b) (c)

(d) (e) (f)

Figure 4.9 Optical micrographs of the evolution of pattern surfaces (w = 5 µm and λ = 500 µm): (a) initial surface, (b) 2 minutes, (c) 3 minutes, (d) 4 minutes, (e) 5 minutes, and (f) 6 minutes.

low area indicate that the pad does not contact the low area, as predicted by the contact mechanics models. Moreover, the boundaries between the high and low features become less distinguishable due to the rounding at the edges. Section 4.2.4 explained this as the high stress concentration around the sharp edges in the early stage of planarization. Similar surface morphology was found in Figs. 4.9 (c), (d) and (e) for polishing time of three, four, and five minutes. Nevertheless, after six minutes of polishing, as shown in Fig. 4.9 (f), the surfaces of both high and low features are roughened. Therefore, the pad is now in contact with both the high and low features and both surfaces are polished.

Figure 4.10 shows the evolution of a different pattern with much larger linewidth, 100 μm, and 0.5 area fraction with 200 μm pitch. The trend of surface evolution is similar to the prior case with small line and area fraction. Few scratches were observed on the low area because large contaminant or agglomerate particles might be transported into the trenches. The particles contact with pad asperities to abrade the surfaces of low features. Additionally, the low area starts to be roughened at about four minutes of polishing, earlier than in the prior case. This implies that the pad contacts the low features in the planarization stage for wider lines, which suggests that pad displacement increases with linewidth. A qualitative comparison between the theoretical prediction and the experimental results of the pad displacement is given in the next section.

4.4.3 Effect of Pattern Geometry. Table 4.2 lists the remaining step-heights of various patterns at different polishing duration. For the features of interest, the process is still in the planarization stage because after six minutes of polishing the step-height is generally larger than twice of the RMS surface roughness, about 10 nm. This can be verified by observation under an optical microscope, which shows that the low features are not polished until the end of polishing. The rate of planarization is defined by the reduction rate of step-height, which indicates how quickly the surface topography can be removed in the planarization process. It is found that the rate of planarization is strongly affected by the area fraction of the pattern and less by the linewidth. For $A_f = 0.5$, the surface was planarized at a rate about 220 nm/min, twice the rate of blanket Cu polishing, at about 100 nm/min. For small A_f of 0.01, the planariztion rate is close to the blanket rate, at about 140 nm/min.

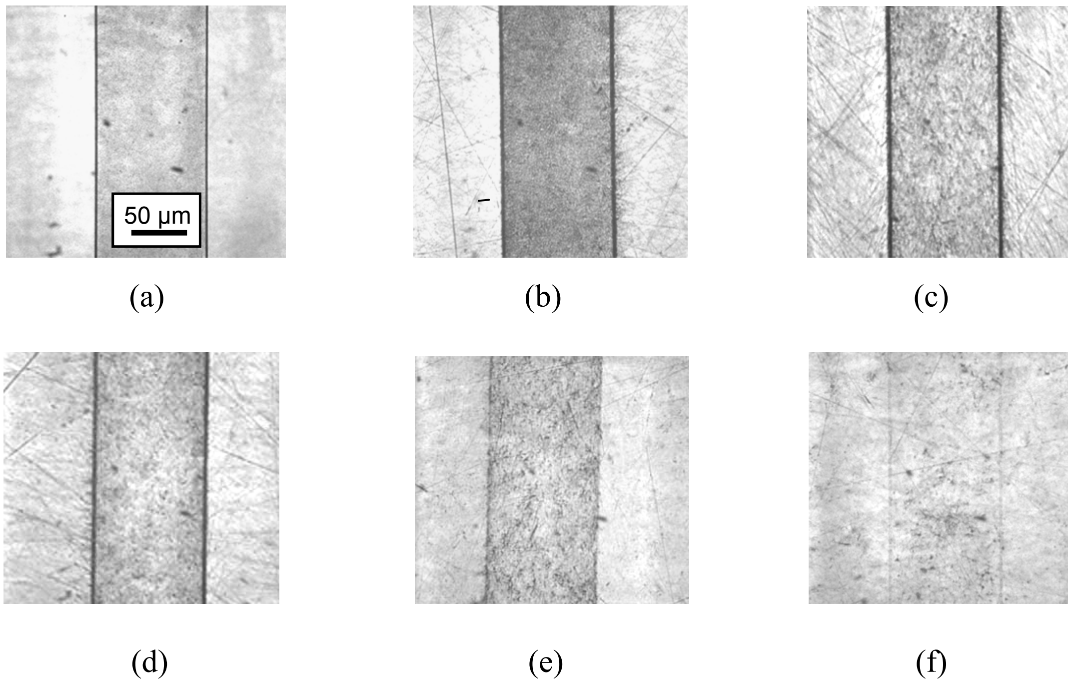

Figure 4.10 Optical micrographs of the evolution of pattern surfaces (w = 100 μm and λ = 200 μm): (a) initial surface, (b) 2 minutes, (c) 3 minutes, (d) 4 minutes, (e) 5 minutes, and (f) 6 minutes.

Table 4.2: Experimental results of step-height evolution at planarization stage.

Linewidth, w (μm)	Pitch, λ (μm)	w/λ	Step-Height at Different Duration (nm)					Rate of Planarization (nm/min)
			2 min	3 min	4 min	5 min	6 min	
2.0	4.0	0.50	857	582	270	114	28	213
2.0	200.0	0.01	800	636	489	355	201	148
5.0	200.0	0.025	851	700	565	315	222	164
5.0	500.0	0.01	849	711	550	435	320	133
25.0	50.0	0.5	897	601	253	47	10	233
25.0	200.0	0.125	795	654	503	321	212	150
100.0	200.0	0.5	945	695	345	78	49	241

Figure 4.11 shows the time evolution of step-heights for patterns with 0.5 area fraction. Again, the high features of 2, 25 and 200 μm line structures were planarized at a similar rate. Since the low area is not polished in the earlier stage of planarization, the MRR at the high feature can be estimated based on the rate of step-height reduction. The dashed line in the figure represents the least square fit of the data before the low area is in contact with pad, which indicates that the MRR on the high features is about 305 nm/min. After about five minutes of polishing, the pad starts contacting the low area when the step-height reaches about 50 to 200 nm, depending on the linewidth of the patterns. The rate of planarization reduces to about 130 nm/min before the surface is planarized, about half that before the pad contacts with low features. This suggests that now the load is uniformly supported by both low and high areas rather than just 50% of the high area as in the earlier stage.

For the wide features, the pad starts to contact the low area much earlier before the topography is planarized. For instance, the low area for the 100 μm line was polished when the step-height was about 350 nm. This step-height is larger than the pad displacement predicted by the contact mechanics model, which is about 20 nm. The low area of a wide feature (interconnect line, contacting pad) will be in contact with the pad at the earlier planarization regime when the size of pad asperities, about 20 – 50 μm, and particle size, about 300 nm, are taken into account. By contrast, for micron or submicron size features, the pad asperities cannot reach the low feature freely with the constraint of the surrounding high features. Hence, the pad does not contact the low area until the end of the planarization regime. Therefore the high feature will be polished further down before the low feature has been polished, as in the case of 2 μm lines.

The high features are removed at a lower rate about 140 nm/min for the first six minutes as shown in Fig. 4.12 for the patterns with 0.01 area fraction and linewidth 2 and 5 μm. The high area is polished slowly because of the small area fraction. Because the removal rate on the high features is low and the linewidth is small, the low area remained unpolished during the polishing period. The MRR on the high area rate is about half that for 0.5 A_f in the earlier planarization stage. These imply that the average pressure on each sub-die is similar. The nonuniformity of material removal rate across a die is essentially due to the non-uniform pressure distribution on the high features affected mainly by the pattern area fraction.

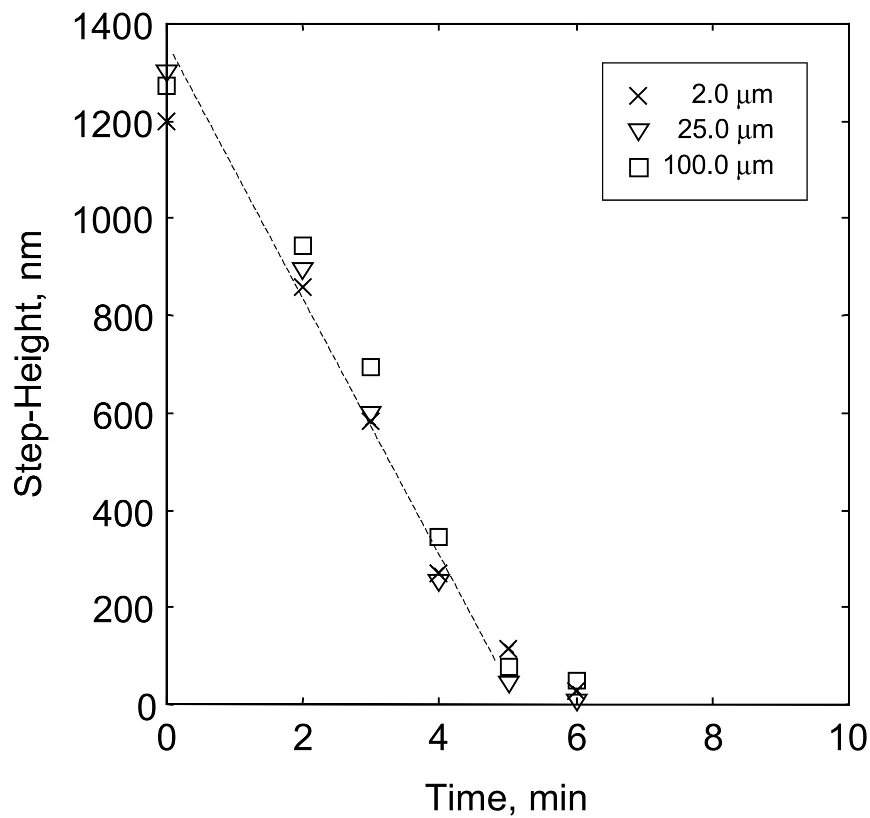

Figure 4.11 Time evolution of step-heights for patterns with constant area fraction 0.5 (w/λ = 0.5) and various linewidths.

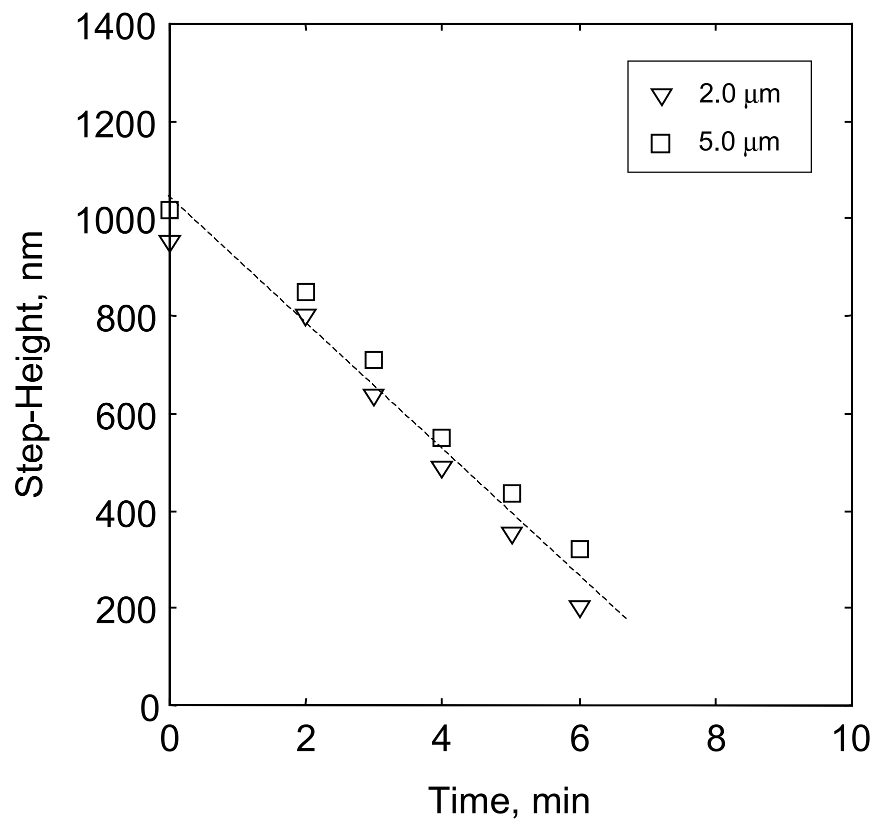

Figure 4.12 Time evolution of step-heights for patterns with constant area fraction 0.01 (w/λ = 0.01) and 2 and 5 μm linewidths.

Moreover, the MRR of high features for the 0.01 area fraction is much higher than the blanket rate. It is slightly higher but close to the blanket rate after the pad is in contact with the low area with uniform pressure distribution. The effects of surface nonplanarity across sub-die areas of different area fractions account for this. The high area fraction area will be planarized faster than the low area fraction. Based on the contact mechanics model, the area of low area fraction will on average support a higher normal pressure. However, compared with a single line, the pressure difference between the high and low area fraction regions usually will not be large because the sub-die area is wide enough for the pad to displace into the low sub-die region to even out the pressure. Additionally, the trenches on the wafer surface might help transport the slurry and thus increase the MRR slightly.

4.5 Conclusions

The planarization behavior in the CMP of Cu patterns was studied based on the contact mechanics models. Experimental results to support the models were presented. Based on the model and the experimental results, the following conclusions are drawn.

(1) Three different boundary conditions: displacement, uniform pressure, and elliptical pressure distribution (Hertzian contact) on high features, were specified to represent initial stage, steady-state stage, and pattern/pad nonconformal situation. For each condition, the pad penetration into low features of sub-micron lines is insignificant compared with the surface roughness of the pad. Therefore, the applied load is carried by the high features during planarization and the MRR increases with the area fraction of Cu interconnects (i.e., the percentage of the low feature area).

(2) Pad displacement increases with the increase of linewidth and area fraction and with decrease of the pad elastic modulus. For the wider Cu features (about 100 μm) at the higher levels of interconnects, the pad may start to contact low area and reduce the rate of planarization and retain the surface topography. For area fraction of about 0.5, the pad displacement does not vary significantly with the area fraction. Additionally, the models can be used to choose the desired elastic modulus of pad to help improve the surface planarity for given conditions (pressure, pattern geometry, etc.).

(3) The contact mechanics models cannot be applied when the surface topography is small, such as at the end of the planarization stage and at the dishing and overpolishing regimes. This is because the boundary conditions of pad roughness and the particle/wafer contact are difficult to use in the models. The MRR on the high features will decrease due to the contact of pad on the low area. On the other hand, the nonuniform pressure distribution across different sub-die are explained by the contact mechanics model. The sub-die area polished slowly can be treated as a wide high feature, which carries higher average pressure than the surrounding sub-dies. The MRR on this sub-die area will be higher to retain the within-die surface planarity.

Nomenclature

A_f = area fraction of metal pattern
a = half linewidth of the metal pattern (m)
C_1, C_2, C_3 = integration constants
h = thickness of the material removed on wafer surface (m)
k_p = Preston constant (m^2/N)
P = load per unit length on a high feature (N/m)
p = normal traction on the wafer surface (N/m^2)
p_o = maximum normal traction on a high feature (N/m^2)
q = tangential traction on the wafer surface (N/m^2)
t = experiment duration (s)
u_x, u_z = normal and tangential displacements of the pad (m)
$\overline{u}_z$ = normalized normal displacement of the pad
v_R = relative linear velocity of wafer (m/s)
w = pattern linewidth (m)
x, y, z = Cartesian coordinates (m)
x_o = position of a datum on the displaced surface of pad (m)
Δh = oxide overpolishing (m)
δ = Cu dishing (m)
λ = pattern pitch (m)
ν = Poisson's ratio
σ_z = normal stress on the pad surface (N/m^2)
τ_{xz} = shear stress on the pad surface (N/m^2)

References

Boyd, J.M. and Ellul, J.P., 1996, "Near-Global Planarization of Oxide-Filled Shallow Trenches Using Chemical Mechanical Polishing," *J. Electrochem. Soc.*, Vol. 143, pp. 3718-3721.

Burke, P.A., 1991, "Semi-empirical Modeling of SiO_2 Chemical-Mechanical Polishing Planarization," *Proc. 1991 VMIC Conf.*, pp. 379-384.

Galin, L.A., 1961, *Contact Problems in the Theory of Elasticity*, translated by Moss, H., Sneddon, I. N., Editor, North Carolina State College, Raleigh, NC.

Chekina, O.G., Keer, L.M., and Liang, H., 1998, "Wear-Contact Problems and Modeling of Chemical Mechanical Polishing," *J. Electrochem. Soc.*, Vol. 145, pp. 2100-2106.

Chen, D.-Z. and Lee B.-S., 1999, "Pattern Planarization Model of Chemical Mechanical Polishing," *J. Electrochem. Soc.*, Vol. 146, pp. 744-748.

Chen, D.-Z. and Lee B.-S., 1999, "Parameter Analysis of Chemical Mechanical Polishing: An Investigation Based on the Pattern Planarization Model," *J. Electrochem. Soc.*, Vol. 146, pp. 3420-3424.

Johnson, K.L., 1985, *Contact Mechanics*, Cambridge University Press., Cambridge.

Murarka, S.P., Steigerwald, J. and Gutmann, R.J., 1993, "Inlaid Copper Multilevel Interconnections Using Plnanarization by Chemical-Mechanical Polishing," *MRS Bulletin*, pp. 46-51.

Ouma, D., Stine, B., Divecha, R., Boning, D., Chung, J., Shinn, G., Ali, I. and Clark, J., 1997, "Wafer-Scale Modeling of Pattern Effect in Oxide Chemical Mechanical Polishing," *Proc. SPIE Microelectronics Mfg. Conf.*, pp. 236-247.

Pan, J.T., Li, P., Kapila, W., Tsai, S., Redeker, F., Park, T., Tugbawa, T., Boning, D., 1999, "Copper CMP and Process Control," *Proc. 4th CMP-MIC Conf.*, pp. 423-429.

Park, T., Tugbawa, T., Boning, D., Hymes, S., Brown, T., Smekalin, K., and Schwartz, G., 1999, "Multi-level Pattern Effects in Copper CMP," *CMP Symposium, Electrochem. Soc. Meeting*, Honolulu, HA, pp.94.

Park, T., Tugbawa, T., Boning, D., Chung, J., Hymes, S., Muralidhar, R., Wilks, B., Smekalin, K., Bersuker, G., 1999, "Electrical Characterization of Copper Chemical Mechanical Polishing," *Proc. 4th CMP-MIC Conf.*, pp. 184-191.

Preston, F.W., 1927, "The Theory and Design of Plate Glass Polishing Machines," *J. Soc. Glass Technology* , Vol. 11, pp. 214-256.

Runnels, S.R., 1994, "Feature-Scale Fluid-Based Erosion Modeling for Chemical-Mechanical Polishing," *J. Electrochem. Soc.*, Vol. 141, pp. 1900-1904.

Runnels, S.R., 1996, "Advances in Physically Based Erosion Simulators for CMP," *J. Electronic Materials*, Vol. 25, pp. 1574-1580.

Smith, T.H., Fang, S.J., Boning, D., Shinn, G.B. and Stefani, J.A., 1999, ”A CMP Model Combining Density and Time Dependencies,” *Proc. 4th CMP-MIC Conf.*, pp. 93-104.

Steigerwald, J.M., Zirpoli, R., Murarka, S.P., Price, D. and Gutmann, R.J., 1994, ”Pattern Geometry Effects in the Chemical-Mechanical Polishing of Inlaid Copper Structures,” *J. Electrochem. Soc.*, Vol. 141, pp. 2842-2848.

Stine, B., Ouma, D., Divecha, R., Boning, D., Chung, J., Hetherington, D., Ali, I., Shinn, G., Clark, J., Nakagawa, O.S., and Oh, S.-Y., 1997, “A Closed-Form Analytic Model for ILD Thickness Variation in the CMP Processes,” *Proc. 2nd CMP-MIC Conf.*, pp. 267-273.

Warnock, J., 1991, “A Two-Dimensional Process Model for Chemimechanical Polishing Planarization,” *J. Electrochem. Soc.*, Vol. 138, pp. 2398-2402.